Electronic Supporting Information

Thermally induced migration of a polyoxometalate within a metal–organic framework and its catalytic effects

Cassandra T. Buru,[a] Ana. E Platero-Prats,‡[b] Daniel G. Chica,[a] Mercouri G. Kanatzidis,[a] Karena W. Chapman,[b] Omar K. Farha[a,c]*

[a] Department of Chemistry, Northwestern University, 2145 Sheridan Road, Evanston, Illinois 60208, USA

[b] X-ray Science Division, Advanced Photon Source, Argonne National Laboratory, Argonne, Illinois 60439-4858, USA

[c] Department of Chemistry, Faculty of Science, King Abdulaziz University, Jeddah, Saudi Arabia

Table of Contents

Section S1. Materials

NU-1000 and PW_{12}@NU-1000-120°C were synthesized according to previously published procedure.[1,2] Phosphotungstic acid hydrate was purchased from Sigma Aldrich, and TGA analysis indicated an average of 24 water molecules were associated with each POM. For NMR comparisons, 2-chloroethyl ethyl sulfoxide (CEESO) was synthesized from 2-chloroethyl ethyl sulfide (CEES) under using NU-1000 catalyst under UV-LED irradiation and 1 atm O_2.[3] The identity and purity were confirmed by GC-MS, ^{1}H NMR, and ^{13}C NMR spectroscopy. All other chemicals were used as received from Fisher Scientific or Sigma Aldrich. All gasses for activation and quantification were Ultra High Purity Grade 5.

Section S2. Physical Methods and Instrumentation

N_2 adsorption and desorption isotherm measurements were performed on a Micromeritics Tristar II at 77 K. To calculate volumetric plots, the density of NU-1000 was reported to be 0.486 cm^3/g [4] and PW_{12}@NU-1000-x were calculated to be 1.0 g/cm^3.

Inductively coupled plasma optical emission spectroscopy (ICP-OES) samples of solids were analyzed with Thermo iCap7600 ICP-OES spectrometer, equipped with a CCD detector and Ar plasma covering 175-785 nm range.

Powder X-ray diffraction (PXRD) patterns were collected on a Stoe STADI-MP instrument using Kα1 Cu radiation. Samples were scanned at 40 kV and 40 mA, a step size of 2θ = 0.015°. For variable temperature measurements, the instrument was equipped with a furnace. The sample was loaded into a capillary, heated at a rate of 20 °C/min to 120 °C, and held at 120 °C for 12 h, then cooled to room temperature.

High resolution powder X-ray diffraction data were collected at beamline 17-BM at the Advanced Photon Source (APS) at Argonne National Laboratory (ANL). The incident X-ray wavelength was 0.45336 Å. Data were collected using a Perkin Elmer flat panel area detector (XRD 1621 CN3/EHS) over the angular range 0.5-9° 2θ. Samples were carefully ground and loaded into 1 mm diameter kapton capillaries. All measurements were performed at room temperature and ambient pressure. Lattice parameters and peak intensities were extracted from diffraction patterns via Le Bail whole pattern fitting[5] using Jana2006,[6] based on the reported structural model for NU-1000 (P6/mmm, a ~ 40 Å, c ~ 17 Å).[4] Lattice and pseudo-Voigt profile parameters were refined over a 0.5-9° 2θ range. Structure envelopes were generated using the intensities of low index reflections.[7] Difference envelope densities (DEDs) were then obtained via subtraction of the envelope for pristine NU-1000 from the envelope for POM@NU-1000.

Solution NMR spectra were collected on a 500 MHz Bruker Avance III system equipped with DCH CryoProbe or on a 400 MHz Agilent DD MR-400 system at IMSERC (Integrated Molecular Structure Education and Research Center) at Northwestern University. Solid-state NMR spectra were collected on a Varian 400 MHz VNMRS system.

Scanning electron microscopy (SEM) images and energy dispersive spectroscopy (EDS) line scans were collected using a Hitachi SU8030 FE-SEM microscope at Northwestern University's EPIC/NUANCE facility. All samples were coated with ~15 nm of OsO_4 or Au/Pd immediately prior to imaging.

GC-FID measurements were carried out on an Agilent Technologies 7820A GC system equipped with an Agilent J&W GC HP-5 capillary column (30 m × 320 μm × 0.25 μm film thickness). All samples were filtered and diluted with dichloromethane prior to injection. Starting temperature: 70 °C, Hold: 0.5 min, Ramp: 30 °C/min, Time: 1 min, Ramp: 75 °C/min, End temperature: 250 °C. The disappearance of the reactant was calculated relative to a 0-minute time point.

Thermogravimetric analyses (TGA) and differential scanning calorimetry (DSC) measurements were performed on a Mettler Toledo STAR^e TGA/DSC 1 under a N_2 flow at a 10 °C/min ramp rate from 25 to 700 °C.

Cyclovoltammograms were recorded with a Solartron Analytical Modulab using a 1 MS/s potentiostat module. The working electrode was made of glassy carbon, the counter electrode was a platinum wire, and the reference electrode was a saturated calomel electrode (SCE). All electrolyte solutions were prepared with de-ionized water. A pH 2.5 H_2SO_4/Na_2SO_4 buffer solution was prepared by mixing 0.5 M Na_2SO_4 solution with H_2SO_4. The solution was deoxygenated with N_2 for 20 min prior to electrochemical measurements. To measure solid PW_{12}@NU-1000-x, the powder was suspended in acetone and drop-casted onto the working electrode.

The steady state emission spectra were measured on a Photon Technology International (PTI) QuantaMaster 400 fluorometer. The samples were excited at 380 nm and emission spectra were monitored between 400 nm to 700 nm.

Diffuse reflectance spectra were collected on a Shimadzu UV-3600 PC double-beam, double-monochromator spectrophotometer in the range of 900 to 250 nm. $BaSO_4$ was taken as the 100% R baseline in the range measured. The powdered sample was firmly pressed on a bed of $BaSO_4$. The reflectance data was converted to absorbance data using the Kubelka - Munk equation: $\alpha/S = (1-R)^2/2R$, where R is reflectance, α is the absorption coefficient, and S is the scattering coefficient.

Section S3. PW_{12}@NU-1000-$scCO_2$ Preparation

In a centrifuge tube, $H_3PW_{12}O_{40}$ (130 mg, 0.04 mmol) was dissolved in 10 mL deionized water. To the solution, NU-1000 (50 mg, 0.023 mmol) was added and suspended by sonicating for about 1 min. The suspension was shaken periodically. After 3 days, the solid was washed with water three times.

Then, the solid was washed with absolute ethanol, allowed to sit overnight in ethanol, and washed two more times with ethanol. The solid from the final wash was suspended in a minimum amount of ethanol and transferred to a glass dish fitted for the supercritical drier. The supercritical drying process used a TousimisTM Samdri PVT-3D critical point drier in which liquid CO_2 was used to exchange ethanol 4 times over 8 h. The material was then heated above 31 °C (P = 73 atm), the critical point of CO_2 before the instrument was evacuated at a rate of 0.1 sccm.[8–10]

Section S4. Additional Characterization

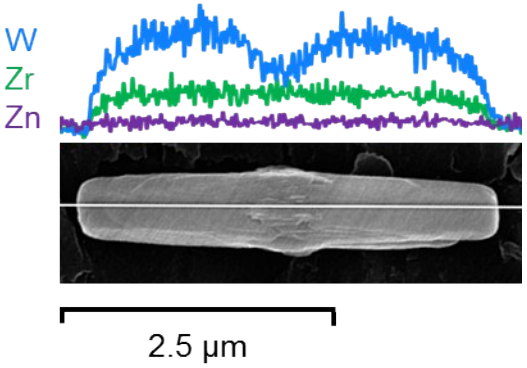

Figure S1. SEM-EDS image and W, Zr, Zn line scans of PW_{12}@ NU-1000-$scCO_2$. Elemental distributions are identical to those found in PW_{12}@NU-1000-120°C.[2] Zn is shown as a baseline.

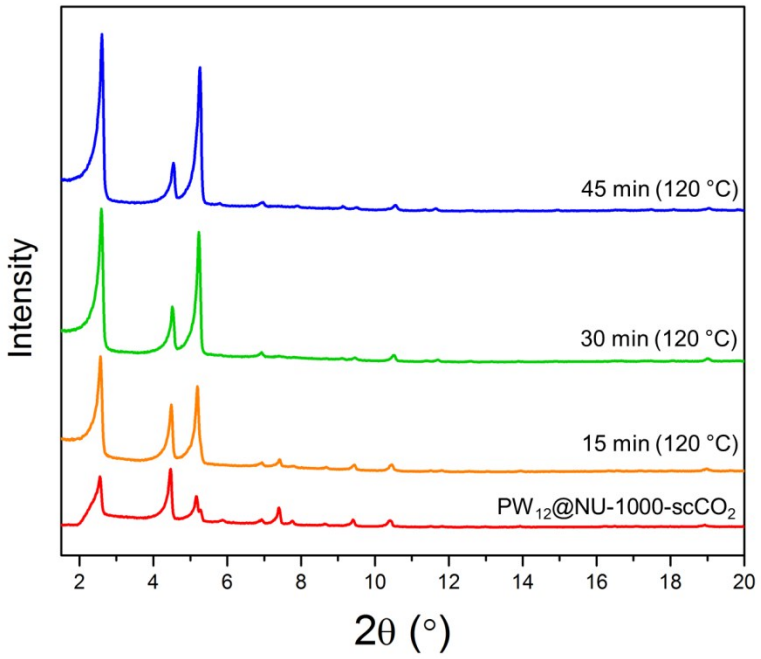

Figure S2. Variable-temperature powder X-ray diffraction patterns for PW_{12}@NU-1000-$scCO_2$ showing dynamic changes in peak intensities as the material is held at 120 °C

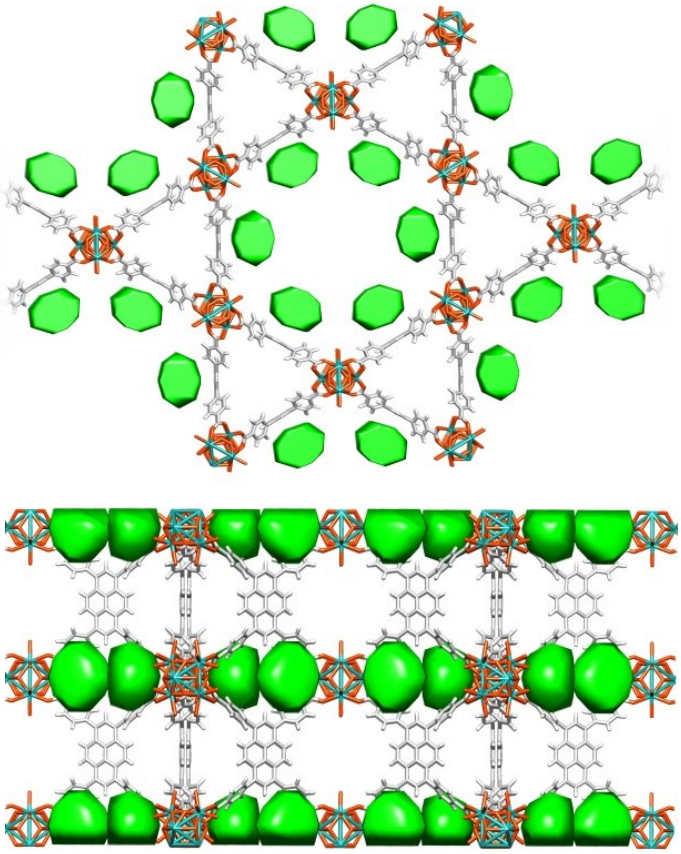

Figure S3. Difference envelope density maps of PW_{12}@NU-1000-scCO_2 derived from experimental ex-situ XRD data collected at 17-BM beamline, APS Room temperature, air atmosphere. Two views are shown: down the c-axis (left) and an orthogonal view (right). Green spheres represent electron density for $[PW_{12}O_{40}]^{3-}$. Teal=Zr, red=O, light gray=C, white=H, hydrogens on the nodes are not shown.

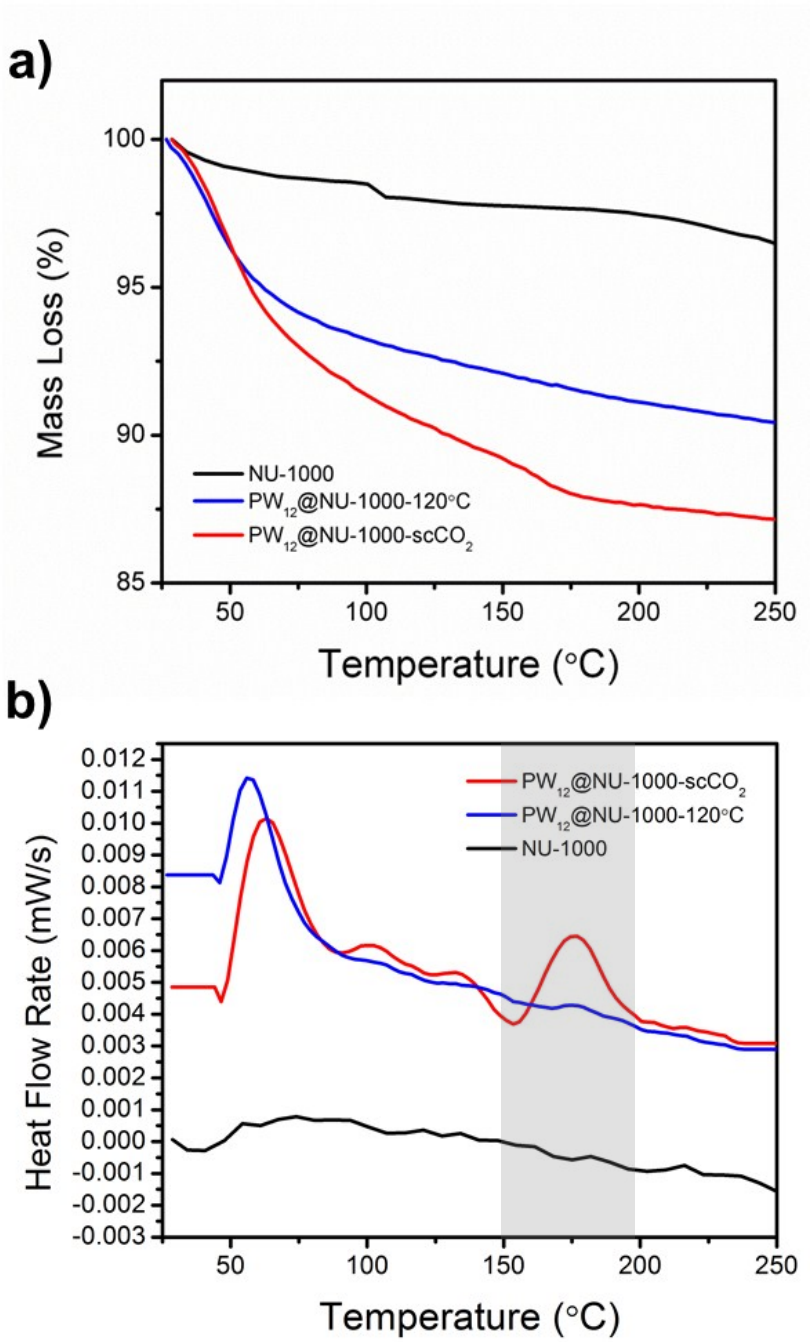

Figure S4. a) Thermogravimetric analysis curve (20 °C /min) showing weight loss of NU-1000, $H_3PW_{12}O_{40}$ and PW_{12}@NU-1000 from 25 °C to 250 °C where water loss occurs and b) differential scanning calorimetry curves which were taken simultaneously. Difference in rate around 175 °C attributed to the movement of the POM from mesopores to micropores. The discrepancy in this transition temperature and the temperature in the in situ PXRD is attributed to the ramp temperature (120 to 175 °C takes less than 3 min).

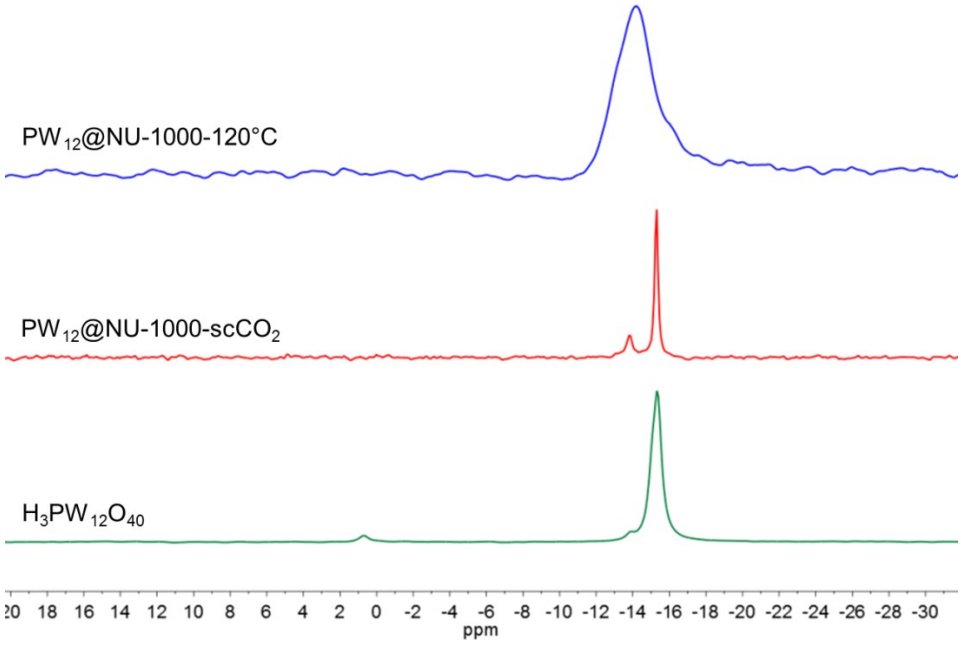

Figure S5. ^{31}P MAS NMR spectra of $H_3PW_{12}O_{40}$ and PW_{12}@NU-1000-x. External reference: 0.8ppm $NH_4H_2PO_4$

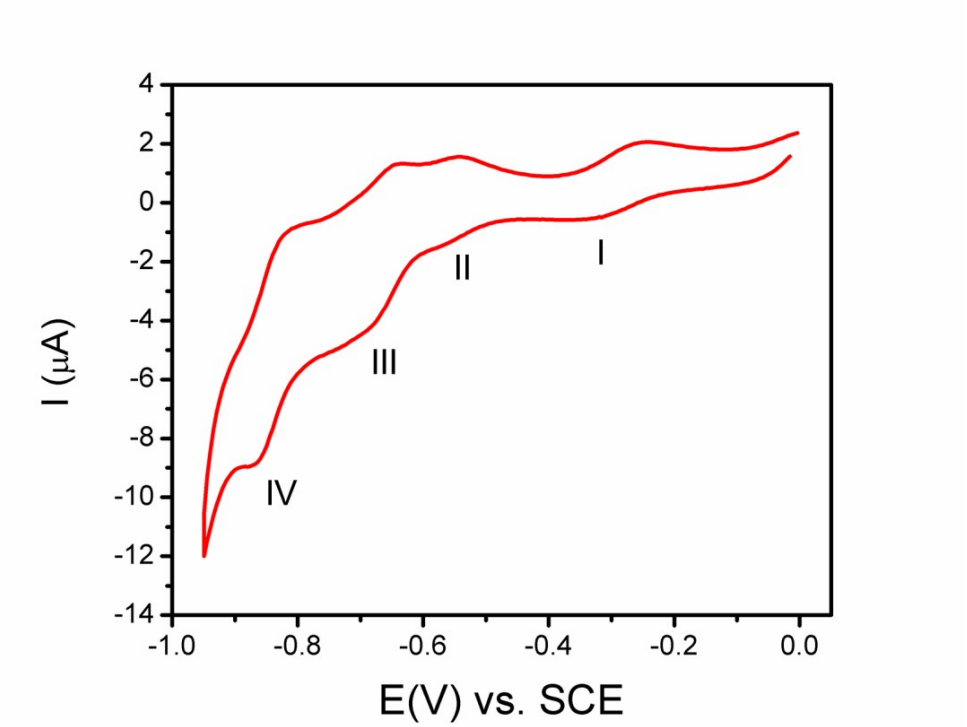

$H_3PW_{12}O_{40}$		-735	-555	-335
PW_{12}@NU-1000-120°C	-890	-715	-560	-300
PW_{12}@NU-1000-$scCO_2$	-840	-670	-555	-285

Figure S6. Cyclic voltammogram of PW_{12}@NU-1000-$scCO_2$ under N_2 in pH 2.5 H_2SO_4/ Na_2SO_4 0.5 M buffer solution at 0.025 Vs^{-1} scan rate. Reductive events labeled. $W^{V/VI}$ reduction events labeled. Formal reduction potentials expressed in mV are listed in the table. The fourth redox event of the POM was obscured by hydrogen evolution.

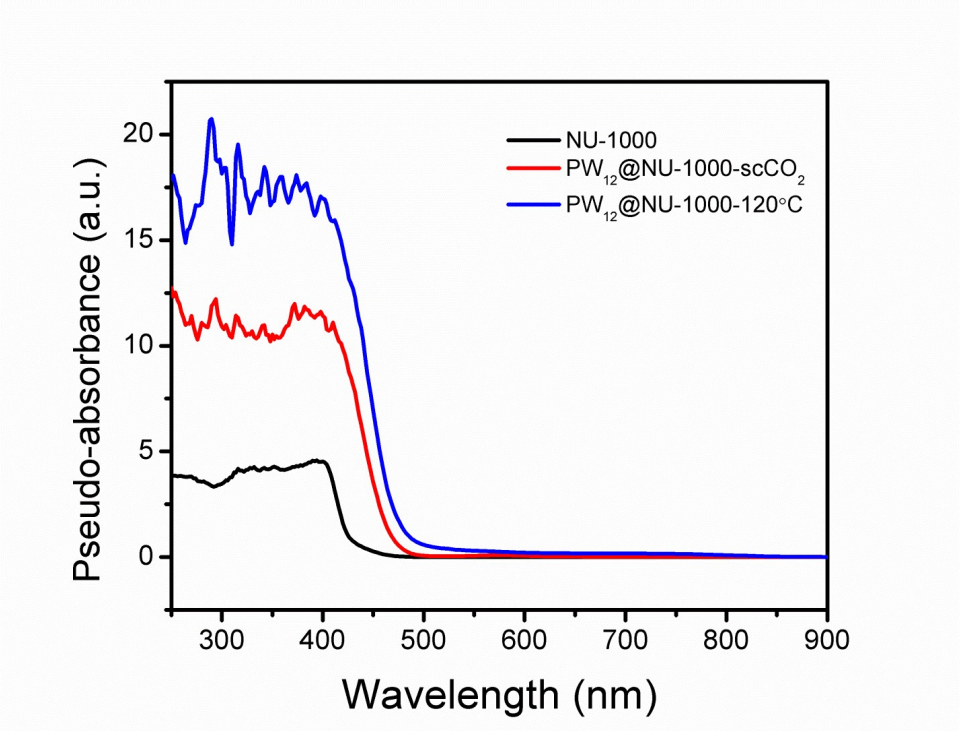

Figure S7. Full diffuse reflectance UV-vis of NU-1000 and PW_{12}@NU-1000-x composites.

Section S4. Catalytic Studies

Procedure

For 2-chloroethyl ethyl sulfide (CEES) oxidation experiments, the catalyst (1.7 μmol of active site) was dispersed in 1 mL of acetonitrile in a 2-dram vial. For the POM and POM@MOF, the water weight was considered, so 1.7 μmol active sites was equivalent to 3.7 mg NU-1000, 5.7 mg $H_3PW_{12}O_{40}$, and 4.7 mg PW_{12}@NU-1000-scCO_2. To ensure the same amount of material was used for PW_{12}@NU-1000-120°C, 4.7 mg PW_{12}@NU-1000-scCO_2 was heated in a 120 °C oven for 2 h prior to catalysis.

CEES (10 μL, 85 μmol) and an internal standard (1-bromo-3,5-difluorobenzene, 5 μL) was added to the reaction vial. Then, hydrogen peroxide (30 wt% in water, 13 μL, 1.5 eq) was added. The vial was placed in a sand bath, which was pre-heated to 45 °C. Aliquots, approximately 10 μL, were withdrawn from the vials with a glass pipette, filtered, and diluted with dichloromethane for GC-FID or deuterated acetonitrile for NMR spectroscopy. GC-FID was used to monitor conversion and NMR spectroscopy was used to determine selectivity.

For leaching studies, PW_{12}@NU-1000-scCO_2 was filtered out around 30 s (approximately 5 min in solvent total) and any remaining reaction was monitored.

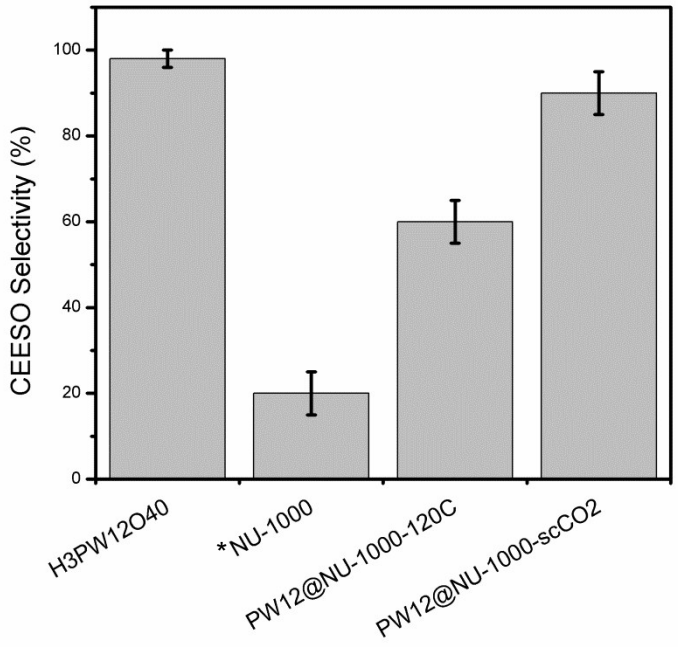

FigureS8. Selectivies for CEESO of the catalysts for the reaction in Figure 5a measured at completion. *When NU-1000 is exposed to enough (5 equivalents) H_2O_2, the reaction is 100% selective for $CEESO_2$.

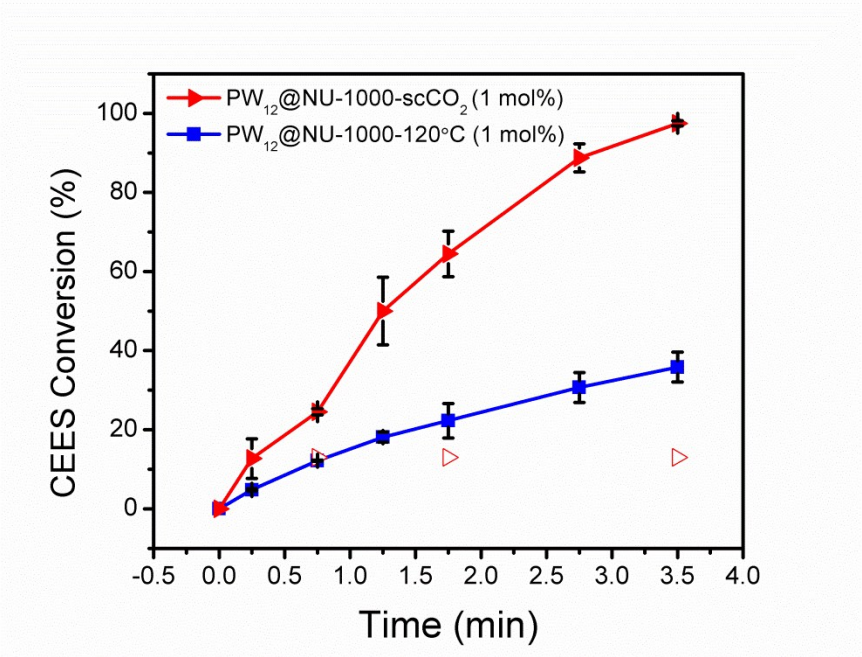

FigureS9. Reaction profiles for the reaction in Figure 5a using only 1 mol% of active clusters with the catalysts PW_{12}@NU-1000-120°C and PW_{12}@NU-1000-$scCO_2$. Open symbols indicate the reaction was filtered at approximately 30 s.

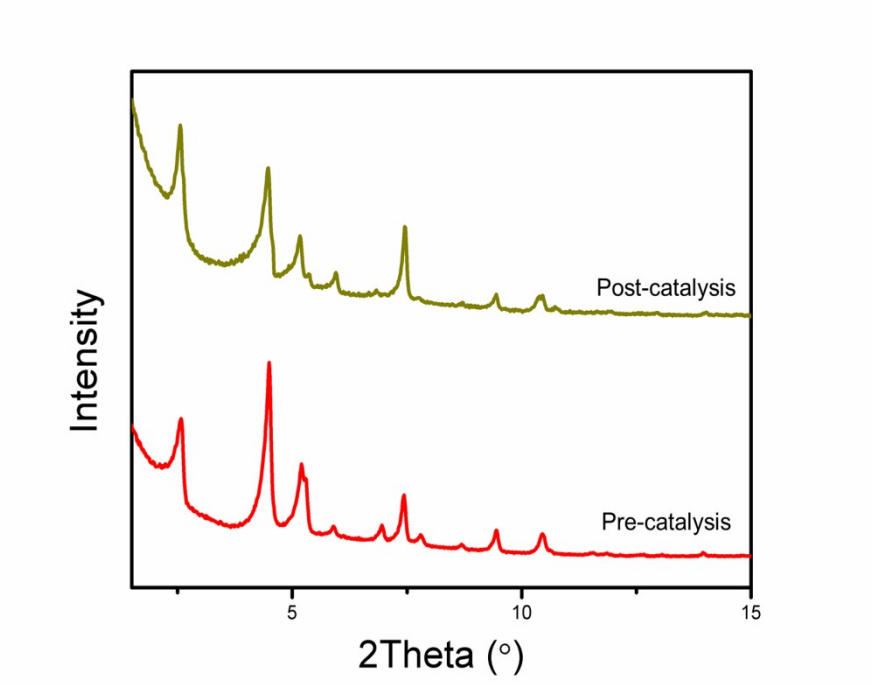

Figures S10. PXRD patterns of PW_{12}@NU-1000-$scCO_2$ before and after catalysis.

Section S5. References

(1) Wang, T. C.; Vermeulen, N. A.; Kim, I. S.; Martinson, A. B. F.; Stoddart, J. F.; Hupp, J. T.; Farha, O. K. Scalable synthesis and post-modification of a mesoporous metal-organic framework called NU-1000. *Nat. Protoc.* **2015**, *11* (1), 149–162.

(2) Buru, C. T.; Li, P.; Mehdi, B. L.; Dohnalkova, A.; Platero-Prats, A. E.; Browning, N. D.; Chapman, K. W.; Hupp, J. T.; Farha, O. K. Adsorption of a catalytically accessible polyoxometalate in a channel-type metal-organic framework. *Chem. Mater.* **2017**, *29* (12), 5174–5181.

(3) Liu, Y.; Buru, C. T.; Howarth, A. J.; Mahle, J. J.; Buchanan, J. H.; DeCoste, J. B.; Hupp, J. T.; Farha, O. K. Efficient and selective oxidation of sulfur mustard using singlet oxygen generated by a pyrene-based metal–organic framework. *J. Mater. Chem. A* **2016**, *4*, 13809–13813.

(4) Mondloch, J. E.; Bury, W.; Fairen-Jimenez, D.; Kwon, S.; Demarco, E. J.; Weston, M. H.; Sarjeant, A. A.; Nguyen, S. T.; Stair, P. C.; Snurr, R. Q.; et al. Vapor-phase metalation by atomic layer deposition in a metal-organic framework. *J. Am. Chem. Soc.* **2013**, *135* (28), 10294–10297.

(5) Le Bail, A.; Duroy, H.; Fourquet, J. L. Ab-initio structure determination of LiSbWO6 by X-ray powder diffraction. *Mater. Res. Bull.* **1988**, *23* (3), 447–452.

(6) Petříček, V.; Dušek, M.; Palatinus, L. Crystallographic Computing System JANA2006: General features. *Zeitschrift für Krist. - Cryst. Mater.* **2014**, *229*, 345.

(7) Yakovenko, A. A.; Reibenspies, J. H.; Bhuvanesh, N.; Zhou, H.-C. Generation and applications of structure envelopes for porous metal-organic frameworks. *J. Appl. Crystallogr.* **2013**, *46* (2), 346–353.

(8) Nelson, A. P.; Farha, O. K.; Mulfort, K. L.; Hupp, J. T. Supercritical Processing as a Route to High Internal Surface Areas and Permanent Microporosity in Metal - Organic Framework Materials. *J. Am. Chem. Soc.* **2009**, *131*, 458–460.

(9) Farha, O. K.; Shultz, A. M.; Sarjeant, A. A.; Nguyen, S. T.; Hupp, J. T. Active-Site-Accessible, Porphyrinic Metal À Organic Framework Materials. *J. Am. Chem. Soc.* **2011**, *133*, 5652–5655.

(10) Shultz, A. M.; Farha, O. K.; Adhikari, D.; Sarjeant, A. A.; Hupp, J. T.; Nguyen, S. T. Selective Surface and Near-Surface Modification of a Noncatenated, Catalytically Active Metal-Organic Framework Material Based on Mn(salen) Struts. *Inorg. Chem.* **2011**, *50*, 3174–3176.